Iranian Journal of Chemical Engineering
Vol. 13, No. 4 (Autumn 2016), IAChE

Simultaneous High Hydrogen Content-Synthesis Gas Production and In-Situ CO_2 Removal via Sorption-Enhanced Reaction Process: Modeling, Sensitivity Analysis and Multi-objective Optimization using NSGA-II Algorithm

M. Heravi[1], M. Bayat[2]*, M. R. Rahimpour[1]

[1]Department of Chemical Engineering, School of Chemical and Petroleum Engineering, Shiraz University, Shiraz 71345, Iran
[2]Department of Chemical Engineering, Faculty of Engineering, University of Bojnord, Bojnord, Iran

ARTICLE INFO

Article history:
Received: 2016-03-10
Accepted: 2016-04-18

Keywords:
Hydrogen Production
Steam-Methane Reforming
Sorption-Enhanced Reaction
CO_2 Adsorption
Multi-objective Optimization

ABSTRACT

The main focus of this study is improvement of the steam-methane reforming (SMR) process by in-situ CO_2 removal to produce high hydrogen content synthesis gas. Sorption-enhanced (SE) concept is applied to improve process performance. In the proposed structure, the solid phase CO_2 adsorbents and pre-reformed gas stream are introduced to a gas-flowing solids-fixed bed reactor (GFSFBR). One dimensional mathematical model is developed to evaluate the effect of adsorbents on the efficiency of SMR at steady-state condition. To prove the accuracy of the considered model, simulation results are compared against available industrial plant data. Modeling results illustrate that application of SE method in SMR enhances syngas production and reduces CO_2 content. The reported data indicate that by overcoming thermodynamic limitations and controlling coke formation, CH_4 conversion and H_2 yield improve about 23 % and 29 %, respectively. For more investigation, sensitivity analyses of some related parameters of the pre-reformed gas are performed to predict optimum conditions. Finally, the proposed GFSFBR for the SMR process leads to higher hydrogen production and H_2/CO ratio. As the last part, non-dominated sorting genetic algorithm-II is applied to perform multi-objective optimization of the SE-SMR.

1. Introduction

Due to the increase in energy demands and the depletion of natural resources, searching for alternative energy sources has recently become an issue of importance. One of the most promising alternative fuels is hydrogen obtained from synthesis gas; synthesis gas is mainly produced by steam-methane reforming

*Corresponding author: m.bayat@ub.ac.ir

(SMR) [1]. This process, which includes the reaction of methane with steam, particularly in the presence of Ni/Al_2O_3 catalyst, occurs at the temperature and pressure range of 400–900 ◦C and 1–30 atm, respectively [2]. Several researchers have studied SMR process from different viewpoints. The studies often include enhancement of H_2 production [3-5].

More important than finding a renewable and non-carbon based energy resource is controlling emissions of greenhouse gases, especially CO_2. This crisis has motivated scientists to find effective methods for CO_2 removal. One of the cost-effective and energy-efficient techniques is CO_2 adsorption in the reactor media called sorption-enhanced reaction (SER) [6]. SER is an effective concept which alleviates thermodynamic limitations of the equilibrium reactions by selectively removing some of the reaction products from the reaction zone, thereby shifting the equilibrium towards higher production and conversion (according to Le Chatelier's principle) [6]. Eliminating the equilibrium limitations of the reactions would considerably reduce the relevant expenses for the separation of non-converted reactants from the products [7]. As a description on earlier works, Westerterp and Kuczynski studied methanol synthesis in a gas-solid-solid trickle bed reactor [7]. They observed conversion increase when methanol adsorbents were added to the system and found reduction of costs and energy consumption in the process. Ding and Alpay investigated the SE-SMR at high temperature both experimentally and theoretically in the presence of CO_2 adsorbents [8]. From their results, it appears that introducing CO_2 adsorbents enhances the process with higher methane conversion. In 2011, SER in steam reforming of ethanol was studied for hydrogen production, and significant increase in hydrogen yield was reported in the presence of appropriate CO_2 adsorbent [9]. However, there are some drawbacks of in-situ CO_2 sorption: the limited capacity of the adsorbent particles, influence of high temperature condition on the adsorbents, and the necessity of continuous and easy regeneration of adsorbents. In this paper, K_2CO_3-promoted hydrotalcite chemi-sorbents are used in a gas-flowing solids-fixed bed reactor (GFSFBR). The adsorbents offer nearly infinite selectivity for adsorbing CO_2.

Recently, our research team has published several papers on the concept of SER by H_2O removal occurring in the GFSFBR for methanol synthesis [10-12]. To the best of our knowledge, this is the first effort in which the SE-SMR process is mentioned in a GFSFBR system in the presence of K_2CO_3-promoted hydrotalcite, and three objective functions are optimized simultaneously. In the GFSFBRs, a solid phase (fine adsorbent particles) and a gas phase are introduced to the packed bed reactors in which catalyst particles are placed, flowing together into the reaction medium in co-current (or counter-current) mode [13]. Because of the GFSFBRs' adsorbents regenerability, which is the main preeminence of these types of reactors over the conventional ones, a regenerator is embedded beside the reactor.

2. Objectives

In this work, the sorption-enhanced reaction

concept is applied to promote SMR process in order to produce higher-purity hydrogen and reduce carbon dioxide emission by introducing CO_2 adsorbents to the system co-currently. A steady state two-phase theory in plug flow regime is developed to analyze the performance of the new configuration of the industrial steam reformer reactor in the presence of the K_2CO_3-promoted hydrotalcite as CO_2 adsorbent. Finally, in order to investigate the superiority of GFSFBR over CR, the results of both reactor configurations are compared. Meanwhile, the operating conditions of GFSFBR configuration are optimized via the multi-objective optimization method to maximize three object functions of CH_4 conversions, CO selectivity and H_2/CO ratio.

3. Process description

3.1. Conventional SMR

Figure 1 indicates a simplified schematic diagram of a steam reforming unit that is principally composed of a reformer and a reactor [14]. The conventional reformer, which was comprised of a hot opening with huge furnace, contains 184 tubes in 4 rows to decrease heat loss and the number of flambeaus. Heat is transferred to the whole length of tubes. In most cases, commercial Ni/Al_2O_3 catalysts, which are vertically packed in tubes, are exposed to reactions medium. The fired furnace supplies the required energy of the system and the heat produced in combustion is transferred to the endothermic steam reforming reactions through furnace flambeaus to produce

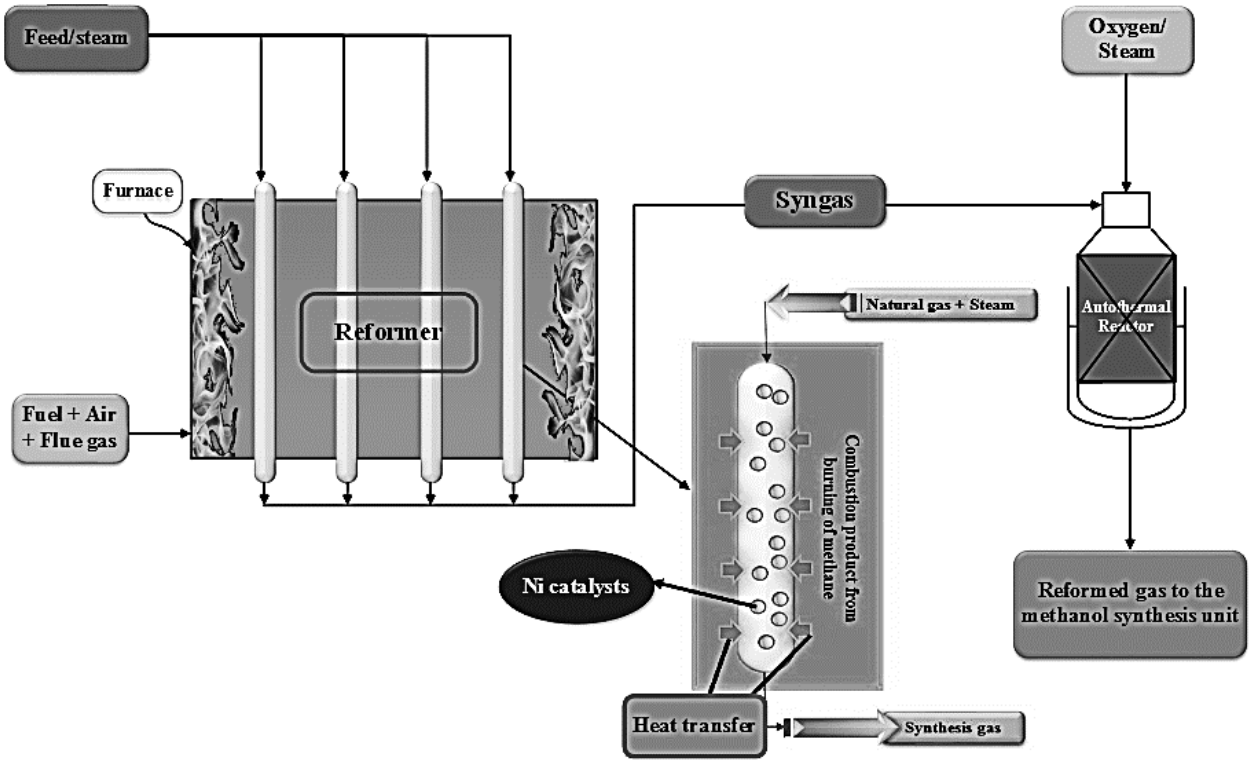

Figure 1. A schematic diagram of the conventional steam reformer reactor (CR) configuration [14].

synthesis gas. As seen, natural gas is first mixed with steam before the gaseous feed enters the tubes of steam reformer and then the SMR reactions are carried out while passing through the fixed bed of catalytic particles in order to produce the final product of syngas. The outlet stream has a relatively high value of H_2/CO ratio that must be adjusted to the optimum value proper for efficient synthesis of methanol. To this end, an autothermal reactor is located downstream of the reformer.

3.2. Proposed structure

In the understudied reactor of the current work, adsorbents, as an additional mobile phase accompanied by gas phase, are fed to the system, flowing along the length of the reactor to reduce CO_2 content of the reaction medium by adsorption mechanism. A schematic of this type of reactor is shown in Fig. 2.

Both the prereformed gas and adsorbents enter the reactor, simultaneously, in order to eliminate thermodynamic limitations of the chemical reactions which are taking over the conventional catalysts through a sorption-enhanced reaction. As mentioned before, adsorbents are regenerated at the end of each adsorption cycle and become fresh in the regenerator so as to be utilized in the next process cycle, introduced at the entrance of the GFSFBR. Continuous regeneration can be enforced applying a proper regeneration technology [15]. Desorbed CO_2 is sent to the methanol synthesis unit. The specifications of the reformer, catalyst and feed composition are available in the literature [16].

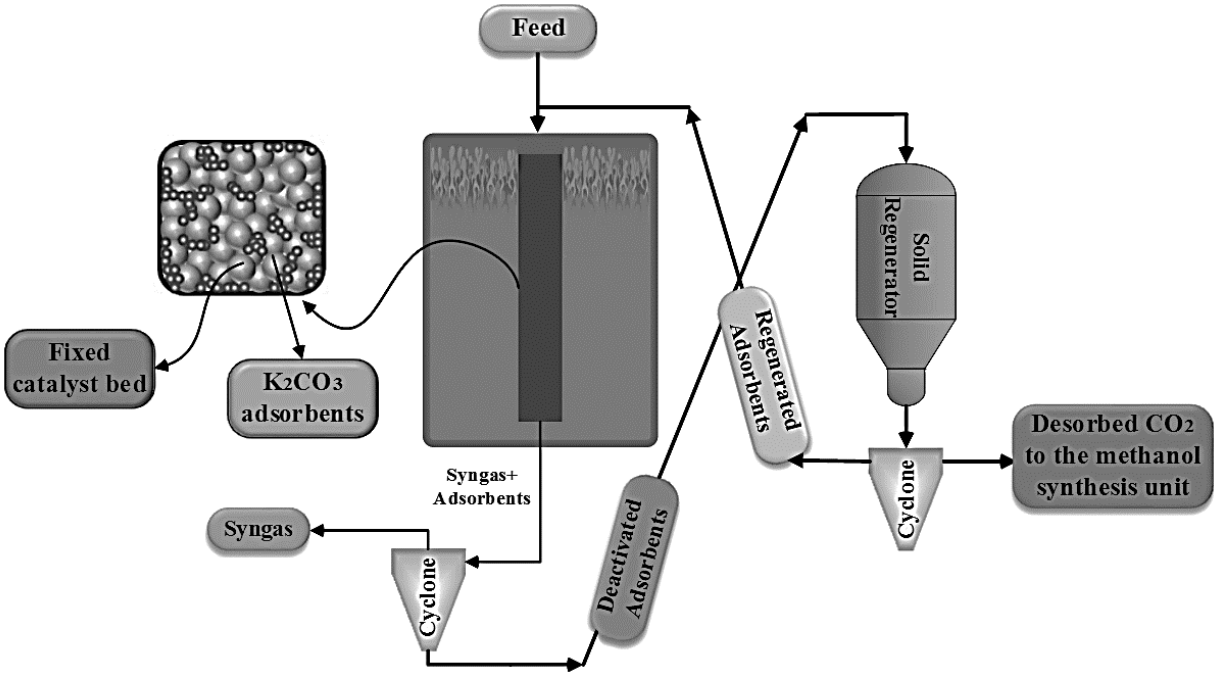

Figure 2. A schematic diagram of multifunctional reactor (MR) for steam-methane reforming process.

4. Reaction scheme and kinetic expression

In this effort, three main reactions considered as the reaction network in steam reformer reactor are presented in Table 1 [17].

The first and the second reactions (1 and 2) are called steam-methane reforming (SMR) reactions through which methane and steam are consumed. The main products of the reaction network are syngas (mixture of CO and H_2) and CO_2. SMR reactions are highly endothermic while the third reaction is slightly exothermic, namely water–gas shift (WGS) reaction. Considering the two endothermic reactions, it is necessary to performed SMR process at high temperatures, which consequently brings about complete methane conversion [16].

Offering a set of approved rate equations is essential to start a mathematical modeling with absolute certainty. Therefore, Xu and Froment model over Ni-based catalyst is applied in this work for predicting the rate of the abovementioned reactions [15]. Arrhenius kinetic parameters, reaction equilibrium constants, and Van't Hoff parameters for adsorption of species are available [16].

5. Mathematical modeling

In this study, a one-dimensional heterogeneous model is developed to investigate the performance of the proposed structure at steady-state condition. The considered assumptions in the developed model are as follows:

- Plug flow pattern is assumed for both gas and flowing solids phases.
- Axial diffusion of heat and mass is negligible as compared with convection.
- Bed void fraction in radial directions is considered to be constant.
- The gas phase is considered to be ideal.
- The total molar flow rate is determined, so as to vary along the reaction pathway.
- Heat loss is negligible.

Based upon the aforementioned assumptions, both mass conservation law and first law of thermodynamics for energy balance were applied over a specified differential element. When time variations of the states are set to zero, the mass and energy balance equations for the bulk gas phase (1 & 2) and the catalyst pellets (3 & 4) are:

$$-\frac{1}{A_c}\frac{dF_i}{dz} + a_s.c_t.k_{gi}(y_{is} - y_i) - \gamma.k'_g.a'_s.\rho'_s\left(q^*_{CO_2} - q_{CO_2}\right) = 0 \quad i = 1,2,\ldots,6 \tag{1}$$

$$-\frac{1}{A_c}Cp_g\frac{d(F_tT)}{dz} + a_s h_f(T_s - T) - h'_f a'_s(T - T'_s) + Q = 0 \tag{2}$$

$$a_s.c_t.k_{gi}(y_i - y_{is}) + \rho_B.\eta_i.r_i = 0 \quad i = 1,2,\ldots,6 \tag{3}$$

$$a_s.h_f.(T - T_s) + \rho_B\sum_{j=1}^{3}\eta_j R_j.(-\Delta H_{f,i}) = 0 \tag{4}$$

Required boundary conditions are: $y_i = y_{i0}$ and $T = T_0$ at $z=0$.

Table 1
Three main reactions in SMR [17].

Equation number	Equilibrium reactions	Standard enthalpy
1	$CH_4 + H_2O \leftrightarrow CO + 3H_2$	$\Delta H_{298} = 206.3\,kJ\,mol^{-1}$
2	$CH_4 + 2H_2O \leftrightarrow CO_2 + 4H_2$	$\Delta H_{298} = 164.9\,kJ\,mol^{-1}$
3	$CO + H_2O \leftrightarrow CO_2 + H_2$	$\Delta H_{298} = -41.1kJ\,mol^{-1}$

The effectiveness factor (η_j) can be found in Gosiewski et al.'s paper [18], where Q is the supplied heat by the reformer furnace. It is noticeable that the value of γ is considered to be unity for CO_2 component and zero for others.

Presenting material and energy balance criteria in this section is completed by considering equations related to the flowing solids as the third phase, over a differential volume. Regarding the fact that the concentration of adsorbed CO_2 is increasing along the reactor, the following equations are added to the developed model:

$$u'_s \frac{dq}{dz} = k'_g a'_s \left(q^*_{CO_2} - q_{CO_2}\right) \quad (5)$$

$$u'_s \rho'_s Cp'_s \frac{dT'_s}{dz} = -\Delta H_{ads} S a'_s \left(q^*_{CO_2} - q_{CO_2}\right) + h'_f a'_s (T - T'_s) \quad (6)$$

In the above equations, q_{CO_2}, describes the concentration of CO_2 in the flowing solids. k'_g, which denotes the mass transfer coefficient between gas phase and the adsorbents, is estimated by the Ranz-Marshall correlation [19]. More importantly, $q^*_{CO_2}$ term that describes the adsorption/desorption isotherm of CO_2 on K_2CO_3 particles is calculated by the following Langmuir isotherm:

$$q^*_{CO2} = \frac{m_{CO2} b_{CO2} P_{CO2}}{1 + b_{CO2} P_{CO2}} \quad (7)$$

The required parameters for the Eqs. (1-7) are available in the literature [8,15,16].

Another differential equation of this section is associated with the pressure drop along the reactor. Several articles have been extensively discussed on the pressure drop and flowing solids hold up of the well-known gas-flowing solids-fixed bed contactors [20-22] due to the fact that the total pressure greatly affects the concentration of reactants in gas-phase reactions. In summary, two main reasons which cause pressure drop in this type of reactor are widely investigated in the literature [23]. The correlation of the pressure drop along the length of GFSFBRs is formulated as follows:

$$\frac{dp}{dz} = -\left(\frac{150}{Re_s} + 1.75\right) \frac{u_g^2 \rho_g}{d_{eq}} \frac{(1-\varepsilon')}{\varepsilon'^3} - \frac{3}{4} \frac{C_d \beta_d \rho_g u_r^2}{d'_s \varepsilon'} \quad (8)$$

Due to the presence of flowing particles, void fraction of the packed bed is corrected which is assigned by ε′. For more explanation of the terms β_d (dynamic holdup), β, and β_s (static holdup) references are presented [23,24]. The following empirical correlations are commonly used to calculate the dynamic and static holdup [23].

$$\beta_d = 9.67 . \text{Ré}_s^{1.123} . Ar^{-0.486} \left(\frac{S^2}{\rho'_s . \rho_g . u_g^2}\right)^{-453} . \left(\frac{d_{eq}}{d'_s}\right)^{-0.647} . \varepsilon^{-0.404} (1-\varepsilon)^{0.726} \quad (9)$$

$$\beta_s = 0.0295 . \beta_d^{0.214} . \left(\frac{d_{eq}}{d'_s}\right)^{-1.82} . \phi^{-2.69} . \varepsilon^{-0.31} (1-\varepsilon)^{1.61} \quad (10)$$

Other parameters of the equation can be simply calculated by the auxiliary correlations.

6. Auxiliary correlations and numerical solution

Eventually, the governing mass and energy balance equations, pressure drop correlation, thermodynamic and kinetic relations are

coupled with the auxiliary correlations. Required correlations are presented in Table 2. Molecular weight and critical volume of the components can be obtained from the literature [31].

In order to achieve concentration, pressure, and temperature profiles along the reactor, the set of ordinary differential equations plus algebraic equations are solved by backward finite difference approximation on a discretized domain, applying Gauss–Newton method.

7. Optimization

In the present work, multi-objective optimization method is applied in order to maximize CH_4 conversion, CO selectivity, and H_2/CO ratio simultaneously. The reason why multi-objective optimization is selected refers to the cost of feed, the cost of the additional

Table 2
Auxiliary correlations to estimate physical properties, mass and heat transfer coefficients.

Parameter	Equation	Reference
Component heat capacity	$Cp_{gi} = a + bT + cT^2 + dT^3$	
Mixture heat capacity	$Cp_g = \sum y_i Cp_{gi}$	
Viscosity	$\mu_{gi} = \frac{C_1 T^{C_2}}{1 + \frac{C_3}{T} + \frac{C_4}{T^2}}$	[25]
	$k'_{gi} = 1.17\,\mathrm{Re}'^{-0.42}_s\, Sc_i^{-0.67} u_g \times 10^3$	[26]
	$\mathrm{Re}'_s = \frac{d'_s(u_g - u'_s)\rho_g}{\varepsilon'\mu}$	
Mass transfer coefficient between gas and solid particles and its related parameters	$Sc_i = \frac{\mu}{\rho_g D_{im} \times 10^{-4}}$	
	$D_{im} = \frac{1 - y_i}{\sum_{i=j} \frac{y_i}{D_{ij}}}$	[27]
	$D_{ij} = \frac{1.43 \times 10^{-7} T^{3/2} \sqrt{1/M_i + 1/M_j}}{\sqrt{2} P (v_{ci}^{1/3} + v_{cj}^{1/3})^2}$	[28]
Drag coefficient	$C_d = \frac{24}{\mathrm{Re}'_s}\left(1 + 0.173\mathrm{Re}'^{0.6567}_s\right) + \frac{0.413}{1 + 16300\,\mathrm{Re}'^{-1.09}_s}$	[29]
Heat transfer coefficient between gas and packing elements	$h'_f = \frac{(Nu \times K_g)}{d'_s}$	
Gas density	$\rho_g = \frac{(P \times Mw_g)}{R \times T}$	
Vapor thermal conductivity	$K_{gi} = \frac{B_1 T^{B_2}}{1 + \frac{B_3}{T} + \frac{B_4}{T^2}}$	[30]
equivalent diameter of packing particles, d_{eq}	$d_{eq} = \frac{6 \times (1 - \varepsilon')}{(a'_s + 4/D_i)}$	
Archimedes number for flowing solid particles, Ar	$Ar = \frac{d'^3_s \rho_g (\rho'_s - \rho_g) g}{\mu^2}$	

furnace fuel, and hydrogen-rich synthesis gas production as a great source of energy [32].

7.1. Multi-objective optimization

Multi-objective optimization (MO) contributes to a set of non-dominated solutions named as a Pareto optimal set [33]. Any solution of this set cannot be regarded as a better or worse solution than the others. A curve called Pareto optimal front connects all points of the Pareto set, in that any point along this curve can be improved if there is a fall-off in at least one of the other objectives.

Among different methodologies for solving MO problems, evolutionary algorithms (EAs) which have become of immense interest for the simple reason of being able to find multiple Pareto optimal solutions, are used in this study [34]. One of the most efficient and famous EAs is non-dominated sorting genetic algorithm-II (NSGA-II) which is characterized by its acceptable convergence of the non-dominated front and appropriate dispersion of solutions [10]. A flowchart of NSGA-II and a brief description of the steps involved in this algorithm can be found in the previous publications [10, 35]. In order to optimize the proposed reactor, four case studies are checked using NSGA-II algorithm and MATLAB programming. Essential information about the parameters of NSGA-II algorithm for case studies is presented in Table 3.

7.2. First case study

In the first case study, working of NSGA-II algorithm was evaluated using two difficult test problems. (1) The Tanaka Test Function (TNK) is a constrained, two-variable, two-objective test problem with discontinuous Pareto front. Objective functions of this test problem are presented below:

$$\begin{cases} Minimize \quad f_1(x) = x_1 \\ Minimize \quad f_2(x) = x_2 \\ C_1(x) = x_1^2 + x_2^2 - 1 - 0.1\cos\left(16\arctan\frac{x_1}{x_1}\right) \geq 0 \\ C_2(x) = (x_1 - 0.5)^2 + (x_2 - 0.5)^2 \leq 0.5 \\ 0 \leq x_1\ , \quad x_2 \leq \pi \end{cases} \tag{11}$$

(2) The Kursawe's Test Function (KUR) is an unconstrained, three-variable, two-objective test problem with a non-convex and discontinuous Pareto front. Objective functions are as follows:

$$\begin{cases} f_1(x) = \sum_{i=1}^{n-1}\left[-10\exp\left(0.2\sqrt{x_i^2 + x_{i+1}^2}\right)\right] \\ f_2(x) = \sum_{i=1}^{n-1}\left(|x_i|^{0.8} + 5\sin x_i^3\right) \end{cases} \tag{12}$$

Where $-5 \leq x_1, x_2, x_3 \leq 5$ are the decision variables.

7.3. Second case study

Seven decision variables are chosen in this optimization: inlet temperature of both gas and flowing solid phases, mass flux and diameter of the adsorbents, pressure, total molar flow rate, and H_2/CH_4 ratio. Each of these variables has specific constraints presented below:

$$773 < T_g < 923 \quad (K) \tag{13}$$

$$773 < T_s' < 923 \quad (K) \tag{14}$$

$$10^{-5} < S < 10^{-3} \quad \left(\frac{kg}{m^2.s}\right) \tag{15}$$

$$200 < d_s < 1000 \quad (\mu m) \tag{16}$$

$$2000 < F_t < 3000 \quad (mol/s) \tag{17}$$

Table 3
Applied parameters in NSGA-II algorithm for case studies.

Parameter name	Case 1	Case 2&3	Case 4
Number of decision variables	2(TNK) and 3(KUR)	7	7
Number of objectives	2	2	3
Population size	500	200	200
Selection strategy	Binary tournament	Binary tournament	Binary tournament
Crossover type	Simulated binary crossover	Simulated binary crossover	Simulated binary crossover
Mutation type	Polynomial mutation	Polynomial mutation	Polynomial mutation
Crossover probability	0.9	0.9	0.9
Mutation probability	0.05	0.05	0.05
Generations	1000	1000	1000

$$30 < P < 50 \quad (bar) \tag{18}$$

$$0 < {}^{H_2}/_{CH_4} < 0.5 \tag{19}$$

The aim of this case study is to maximize two objective functions of CH_4 conversion (OF_1) and H_2/CO ratio (OF_3) simultaneously. Therefore, Eqs. 13 and 14 are considered to calculate OF_1 and OF_3.

Maximize: OF_1= CH_4 conversion (%) =

$$\left(\frac{mol\ HC_{in} - mol\ HC_{out}}{mol\ HC_{in}}\right) \times 100 \tag{20}$$

where HC represents hydrocarbon.

Maximize: $OF_3 = \frac{H_2}{CO} = \frac{mol\ H_{2\ out}}{mol\ CO_{\ out}}$ (21)

For the purpose of automatically deleting unacceptable results, a penalty function method is applied with the penalty parameter of 10^7.

7.4. Third and fourth case studies

According to the second case, simultaneous maximization of CO selectivity (OF_2) and H_2/CO ratio (OF_3) is performed in the third case study. Related equations are as follows:

Maximize: OF_2 = CO selectivity (%) =

$$\left(\frac{mol\ C_{out}}{\Sigma mol\ of\ j_{out}}\right) \times 100 \tag{22}$$

Where j = CO, CO_2, H_2, H_2O and CH_4

Maximize: $OF_3 = \frac{H_2}{CO} = \frac{mol\ H_{2\ out}}{mol\ CO_{\ out}}$ (23)

Finally, in the fourth case study all three objectives are considered simultaneously.

8. Model validation

To check the validity of the mentioned model, a comparison between the proposed model for the adsorbents' mass flux of zero (S=0 ${}^{kg}/_{m^2.s}$) and plant data has been established in Table 4. Obviously, the predicted results do not significantly deviate from the output data of the plant. This assertion is proved by the negligible calculated absolute errors presented in the table.

9. Results and discussion

As previously expressed, the aim of this work is to propose an economic and environmentally friendly reformer which increases hydrogen production and decreases the level of carbon dioxide. To reach this goal, the effect of some key parameters on the reformer performance is checked in specified intervals. Simulation results are subsequently

Table 4
Model validation of the SMR process in MR (Outlet conditions) [16].

Parameter	Plant	MR (S=0)	Error %
Temperature (°C)	710	727	+2.39
CH_4 (mol %)	20.41	20.42	+0.049
CO_2 (mol %)	5.71	5.6	-1.93
CO (mol %)	3.15	3.26	+3.49
H_2 (mol %)	31.39	31.26	-0.41
H_2O (mol %)	38.05	38.18	+0.34
N_2 (mol %)	1.29	1.3	+0.77
Methane conversion %	26.5	26.5204	+0.077

compared with those of the conventional SMR model. Finally, the effect of various operating conditions on the behavior of the flowing gas phase is discussed in the remaining subsections.

9.1. Effects of the mass flux and diameter of the adsorbents on components

In this section, the effects of both mass flux and diameter of the adsorbents on the reactions are investigated. In this regard, two terms are introduced by the following formulas:

$$CH_4\ Conversion = \frac{F_{CH4,intlet} - F_{CH4,outlet}}{F_{CH4,inlet}} \quad (24)$$

$$H_2\ Yield = \frac{F_{H2,outlet} - F_{H2,inlet}}{F_{CH4,inlet}} \quad (25)$$

Figure 3 (a-e) illustrates the comparison of methane conversion percentage, H_2 yield and CO_2 molar flow rates in the conventional reactor (CR) and the GFSFBR in two different mass fluxes of flowing solids of 0.001 and 0.01 $kg/m^2.s$. It should be mentioned that the adsorbent diameter is fixed on 200 microns. Figure 3 (a) clearly shows that decreasing CO_2 content over the catalysts surface increases CH_4 conversion in the proposed reactor, compared to the conventional process. Indeed, when CO_2 is removed by adsorbents, the equilibrium reactions are shifted toward more methane consumption, which subsequently leads to a rise in CH_4 conversion. In fact, an increase in the solid mass flux brings about an increase in the adsorbent presence. As a numerical report, at solid mass fluxes of 0.001 and 0.01($kg/m^2.s$), methane conversion increases by about 17.61 % and 23.2 %, respectively.

Figure 3 (b) is an illustration of hydrogen yield throughout the reactor length at different adsorbent mass fluxes. The GFFBR generally enhances the formation of desired product. However, at the entrance of the GFSFBR, adsorbents have negligible influence on the process performance in terms of hydrogen yield. Thus, GFSFBR operates nearly the same as CR because of the short contact time between both moving phases. Two different mass fluxes of 0.001 and 0.01($kg/m^2.s$) show 22 % and 29 % increase in hydrogen yield, respectively.

A comparison of the CO_2 molar flow rate along the GFSFBR and CR is presented in Fig. 3 (c). As seen, utilization of higher solids mass fluxes reduces the CO_2 molar flow rate along the GFSFBR as a result of higher quantities of adsorbents. In summary, mass

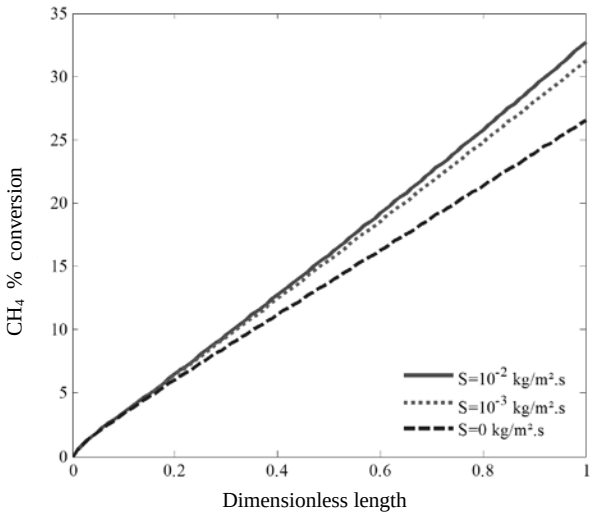

(a)

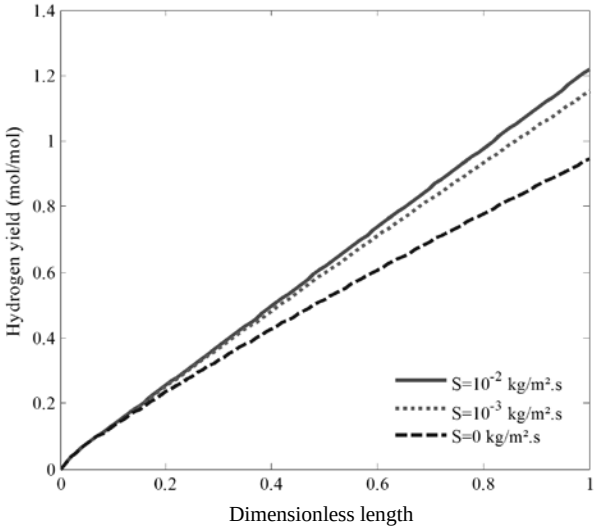

(b)

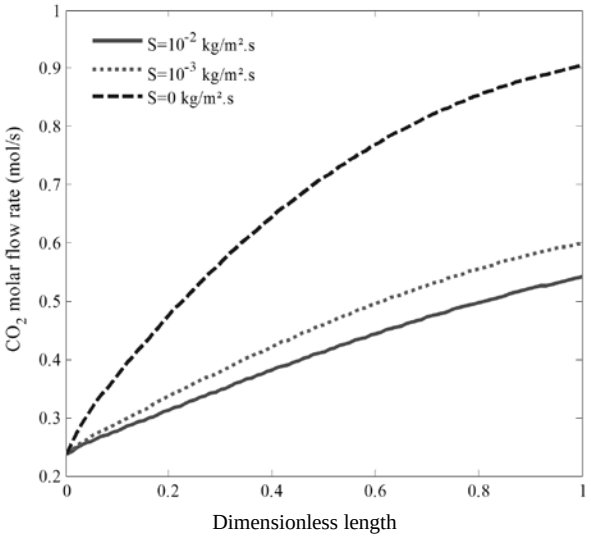

(c)

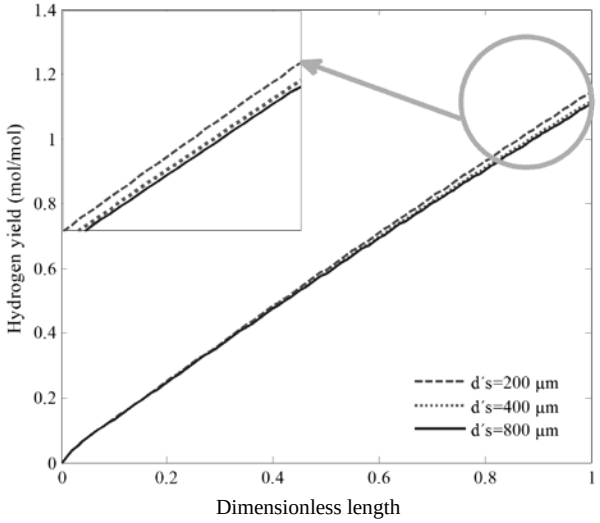

(d)

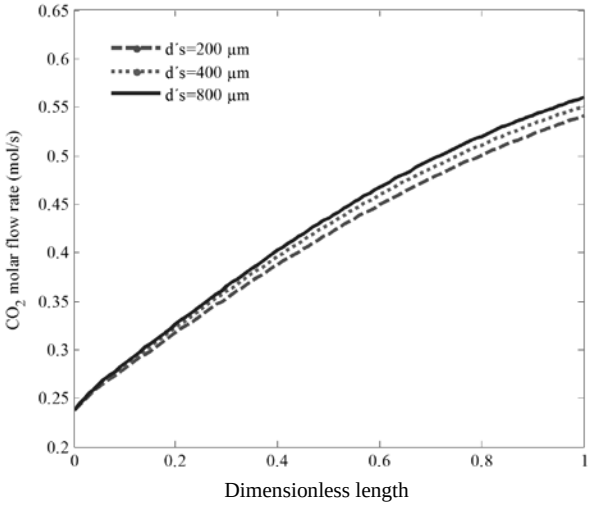

(e)

Figure 3. Comparison of (a) CH_4 conversion, (b) H_2 yield, (c) CO for S=0, 10^{-4}, 10^{-3}, 10^{-2} kg/(m^2.s) and (d) H_2 production and (e) CO_2 molar flow rate for d_s'= 200,400,1000 and 1400 μm between CR and MR .

flux of 0.01 $kg/m^2.s$ is more suitable in the mentioned interval owing to the higher hydrogen yield and methane conversion as well as lower CO_2 molar flow rate.

Analyzing effect of adsorbents diameters is also added to the research. Three different solid diameters are applied to the model in the

interval of 200 to 800 microns. It should be noted that solid mass flux is chosen to be 0.01 $kg/m^2.s$. Results from this trial can be seen in Fig. 3(d-e).

These figures reveal that as solid particles become smaller, H_2 production rate increases and CO_2 molar flow rate decreases which proves adsorption improvement. The main reason of much adsorption is the increase in the contacting surface area between the adsorbents and gas phase in smaller particle sizes.

9.2. Effects of the mass flux and diameter of the adsorbents on pressure and temperature

In this section, the variation of temperature and pressure are discussed owing to their central role in the behavior of SMR reactions. Actually, the rate constants of the SMR reactions are a function of temperature and the rate equations of these reactions are influenced by partial pressure of the components.

As mentioned above, smaller size and higher mass flux of the adsorbents are likely to improve the performance of the reactor. Despite major advantages of any scientific phenomenon, it seems that the possibility of some disadvantages is inevitable. According to Fig. 4(a) and (b), the pressure drop along the GFSFBR length increases in comparison with CR. First, the adsorbents mass flux is kept constant and the GFSFBR operated at different adsorbents diameters. In the next step, a constant particle size of 200 microns was chosen and the mass flux varied (0.001 and 0.01 $kg/m^2.s$). The results clearly represent that the smaller the particle size or the greater the mass flux of flowing solids to the reactor, the higher the bed resistance, which further results in an increase in drag forces. Consequently, the pressure drop increases through the column.

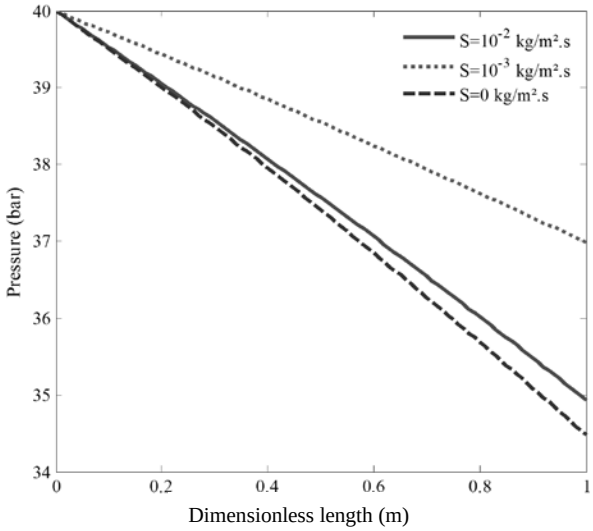

(a)

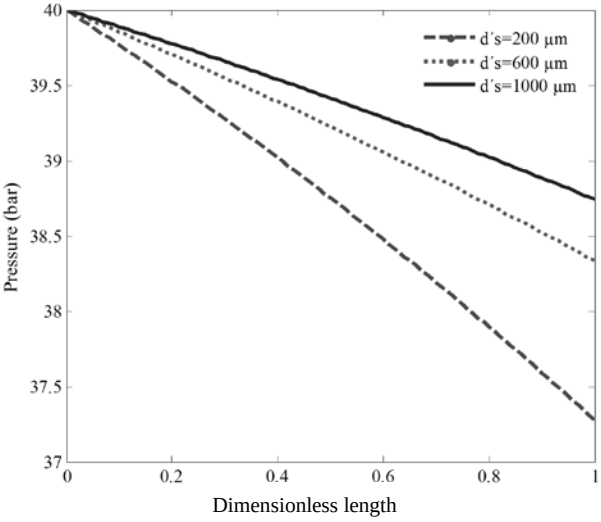

(b)

Figure 4. Gas phase pressure along the MR length for (a) S=0,10^{-4},10^{-3} and 10^{-2} kg/(m^2.s) and (b) d_s'= 200,400,1000 and 1400 μm.

As discussed previously, utilization of higher mass fluxes or smaller diameters of the adsorbents reduce the carbon dioxide molar flow rate along the GFSFBR, which is in association with higher adsorption. Actually, smaller solid particles provide a better contact between the gas phase and surface area of the solids, and higher solid mass fluxes enhance the rate of CO_2 adsorption. As a result, higher methane conversion and subsequently higher required heat of reaction of the two first endothermic reactions is expected. Thus, a reduction in overall heat of reaction network is observed in spite of more heat of adsorption being released inside the reactor; however, in the meantime, an increase in the energy demand for the endothermic reactions overcomes the released energy which eventually causes temperature decrease. It is important to stress that the temperature reduction itself benefits from the adsorption strength of the sorbents. This is depicted in Figure 5 (a-b) in which the lower temperature profiles are observed as the solids mass flux increases or solids particle size decreases. In addition, it is concluded from the figures that the size of particles has only slight impacts on the temperature profiles. What is more, gas phase temperatures in the outlet of the GFSFBR are about 993.3, 999.7 and 1001(K) for adsorbent diameters of 200, 400 and 800 microns, respectively, which proves that the effect of the particle size on temperature is negligible in larger diameters. This fact is also observed in Fig. 5 (e) as the profiles of CO_2 molar flow rates are almost identical.

9.3. Effect of the GFSFBR configuration on H_2, CO, and CO_2

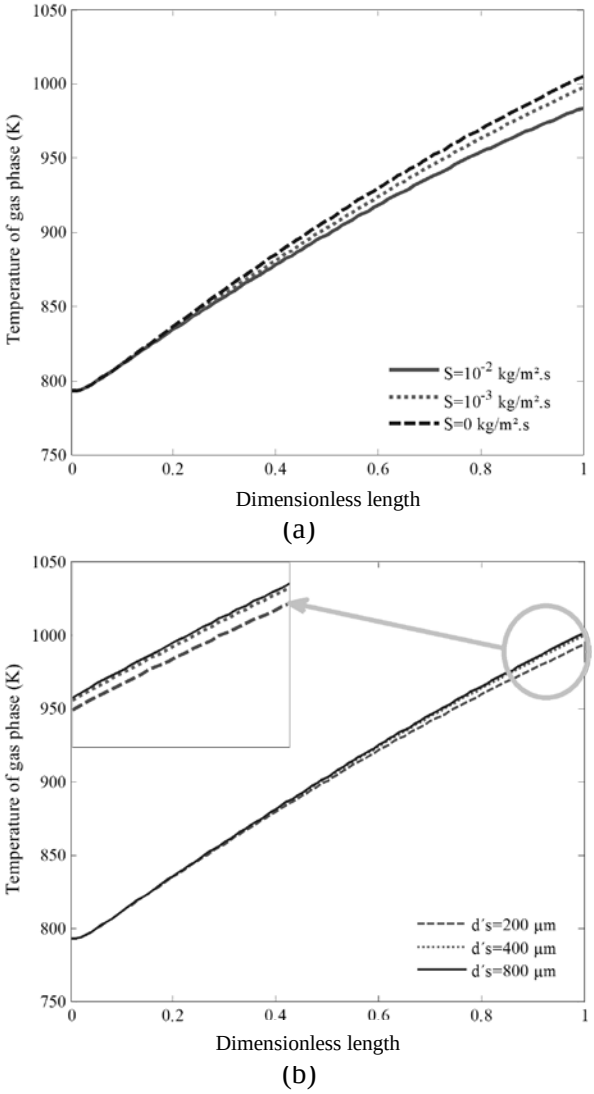

Figure 5. Gas phase temperature along the MR length for (a) S=0,10^{-4},10^{-3} and 10^{-2} kg/(m^2.s) and (b) d_s' = 200,400,1000 and 1400 μm.

According to the above-mentioned figures, with adsorbents' mass flux of 0.01 $kg/m^2.s$ and diameter of 200 microns, the molar flow rates of hydrogen and carbon dioxide, as the major components of this process, are plotted together in Fig. 6. This comparative figure vividly illustrates that the amount of produced H_2 and adsorbed CO_2 significantly increases in GFSFBR configuration. Since hydrogen

can also be utilized as a clean fuel, any increase in its production is favorable. Furthermore, the reduction in CO_2 emission to the atmosphere is an environmentally friendly phenomenon.

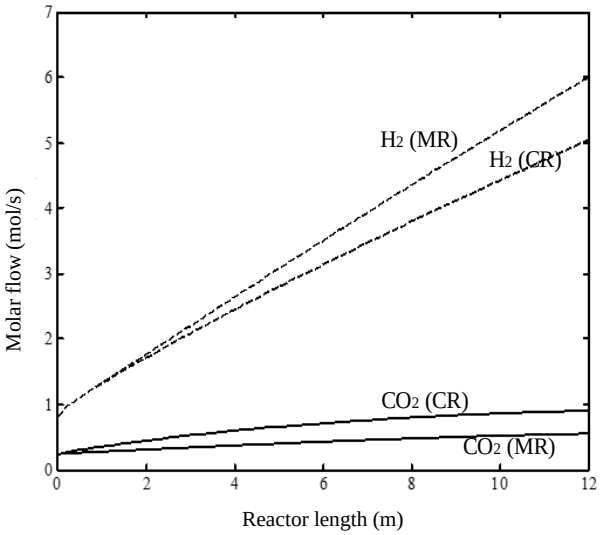

Figure 6. Comparison of H_2 and CO_2 molar flow rates in CR and MR (S=0.01 kg/(m^2.s) and d_s'= 200 μm).

Figure 7 shows a graph of the ratio of hydrogen to carbon monoxide as an important term in the reforming process. It is believed that, the higher the ratio of H_2/CO, the more favorable the system performance due to the higher hydrogen production rate with respect to that of carbon monoxide. The ratio increases about 47 % in GFSFBR owing to the adsorption which is desired for downstream units, especially methanol synthesis unit.

9.4. Effects of the inlet temperature of the gas phase

In this section, investigating the effects of a wide variety of parameters including the inlet temperature, pressure and the total flow rate on the adsorption capability have been taken into account. In this regard, possible advantages of the concept are discussed in terms of methane conversion as well as CO_2 and H_2 flow rate profiles along the GFSFBR reactor.

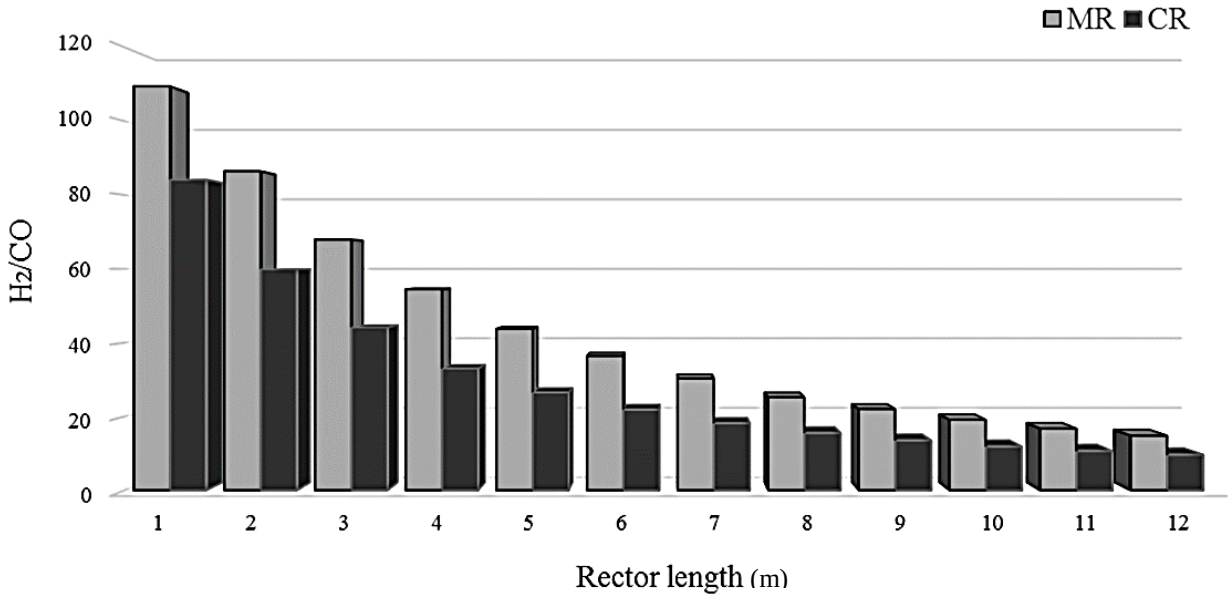

Figure 7. Comparison of H_2/CO ratio in CR and MR configurations (S= 0.01 kg/(m^2.s) and d_s' = 200 μm).

Figure 8 (a-c) depicts 3-D schemes of the influence of the flowing feed temperature on the above-mentioned parameters.

As the temperature increases, more energy is transferred to the reaction zone leading the endothermic reactions of (1) and (2) to a forward direction. As a result, CH_4 conversion as well as H_2 and CO_2 flow rates increase. As known, it is not suitable for the system to produce a higher amount of CO_2. The problem is relatively modified by the WGS reaction that is exothermic in nature. Therefore, the slope of CO_2 rise is slight.

As reported in Table 2, the temperature of 790 (K) is chosen to be the base case in the current study. According to Fig. 8(a), increasing the temperature of the prereformed gas stream to a sufficiently high value of 900 (K), the conversion enhances by about 19 %, that is highly acceptable. Moreover, at higher temperatures, the slope of conversion variation is steeper at the entrance region of the reactor that further results in an immediate conversion of the reacting components. Subsequently, in order to attain specific conversion percentage shorter reactor length is required. This statement is confirmed quantitatively by 22 % reduction in the length of the reacting tubes at 900 (K) with respect to the best case.

Conversion enhancement implies higher hydrogen production rates, a phenomenon that is represented by Fig. 8(b). A trend similar to that of CH_4 conversion is observed by the 3-D graph.

Thereupon, temperature rise is dramatically desirable for H_2 production rate. It is noteworthy that the temperature rise is not in favor of the adsorption. Thus, to promote the SMR process, it is suggested to increase the inlet temperature of the bulk gas phase to an optimum value in which CO_2 desorption is negligible.

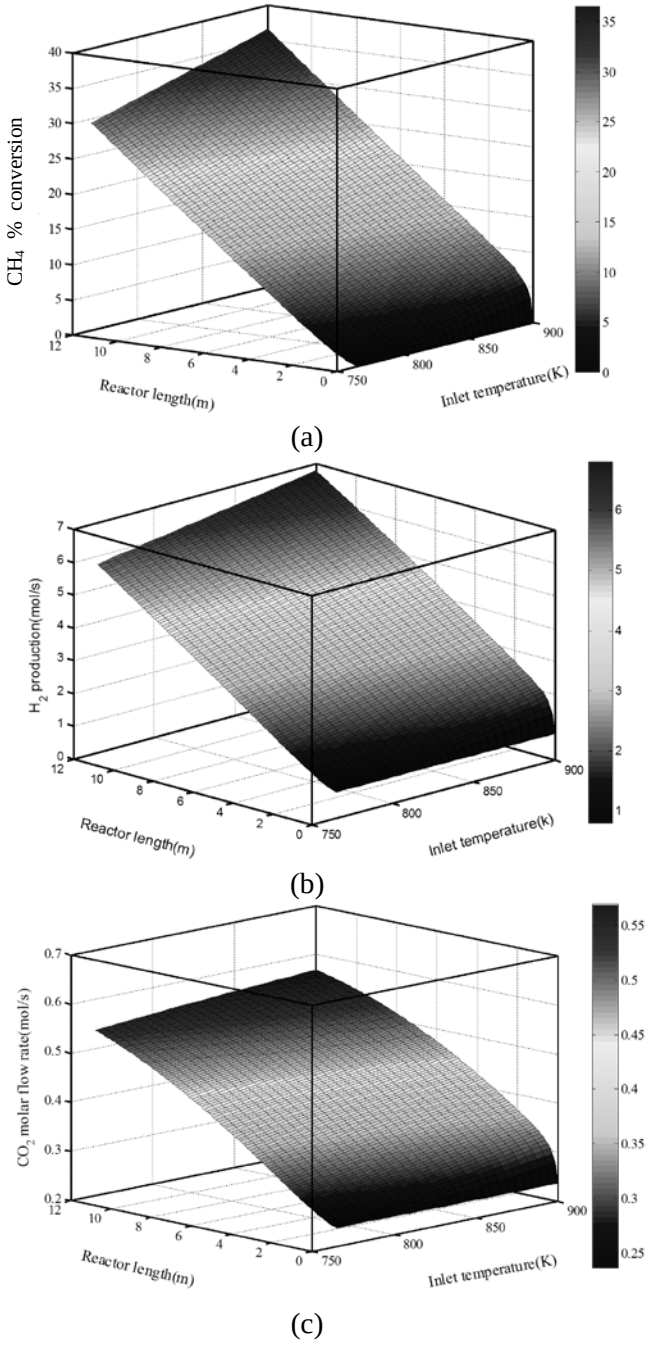

Figure 8. (a) CH_4 conversion, (b) H_2 production and (c) CO_2 molar flow rate along the MR length in different inlet temperatures.

9.5. Effects of the inlet pressure of the gas phase

The profiles of CH_4 conversion, H_2 production rate, and CO_2 molar flow rate are plotted versus the length of the reactor in the pressure range of 35 to 45 bar (Fig. 9 a-c). According to Le Chatelier's principle, Eqs.1 and 2 occur in reverse direction by increasing the pressure, leading to CO, H_2, and CO_2 consumption through the first and second SMR reactions. It is noticeable that the pressure variation does not affect the WGS reaction owing to the molar equality of the reactants and products. All the same, the reduction of CO production through Eq.1 is responsible for the lower amounts of H_2 and CO_2 production in Eq.3 (because it is one of the reactants in Eq.3). Therefore, both CO_2 and H_2 production decrease by the ascension of the pressure. On the other hand, according to Eq.10, the in-situ removal of CO_2 by the adsorption mechanism is improved by increasing the pressure. Consequently, Eqs 2 and 3 are forced to take place in their forward direction that leads to higher H_2 production. However, according to the stoichiometry of the reaction network, the competition between the adsorption phenomenon and Le Chatelier's principle finally causes a reduction in both H_2 and CO_2 flow rates (see Figs. 9(b) and 9(c)).

9.6. Effects of the inlet flow rate of the gas phase

The flow rate variation is also implemented in the model to determine possible effects on the process. Results are shown in 3-D plots of Fig. 10(a-b).

As expected, increasing the inlet flow rate

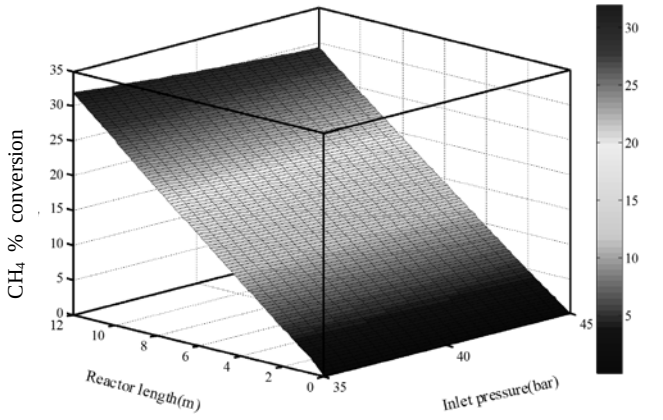

(a)

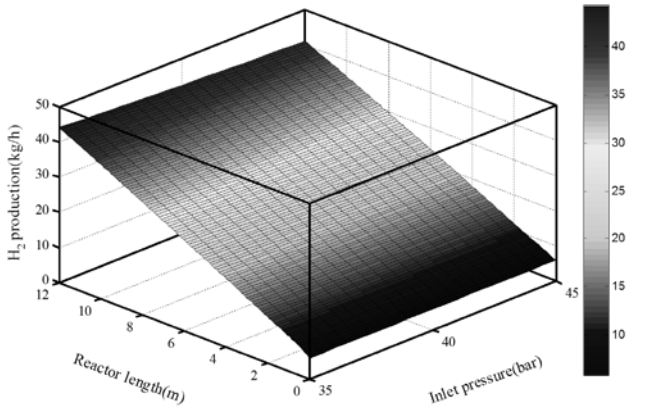

(b)

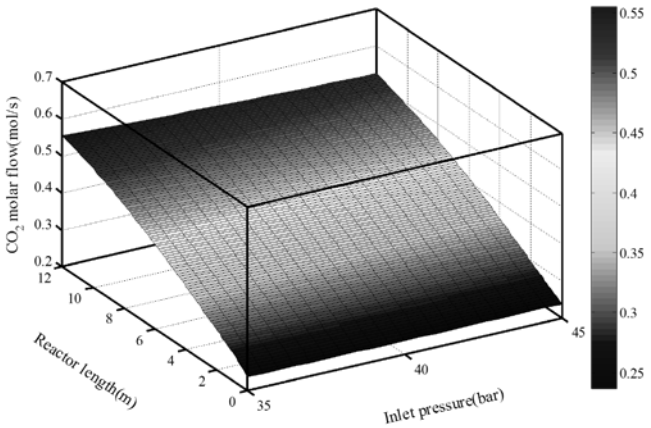

(c)

Figure 9. (a) CH_4 conversion, (b) H_2 production and (c) CO_2 molar flow rate along the MR length in different inlet pressures.

of the gas phase induces shorter residence time. Hence, the collision occurs in an insufficient period of time, resulting in inefficient collision between catalytic spheres and prereformed gas molecules. Accordingly, the reduction in the conversion of methane that is shown in Fig. 10 (a) is predictable. Taking a closer look at the graph, it can be understood that the influence of the feed flow rate on the conversion is considerably greater at lower amounts.

Additionally, the shorter residence time has another effect in terms of CO_2 adsorption through K_2CO_3 (see Fig. 10(b)). The curvature that appears in the figure is due to the fact that sorbents are fresh at first, providing a higher driving force to adsorb CO_2. Therefore, the concentration of the adsorbed CO_2 is rising. But this increasing trend stops when sorbents become saturated according to the Langmuir equivalent adsorption model. At this point, sorbents are incapable of adsorbing further CO_2 and need to be regenerated. The saturation point occurs when the adsorbents pass approximately 60 % of the total reactor length. Afterwards, the GFSFBR operates similar to the CR. Also, the increase in the feed flow rate decreases the strength of adsorption negligibly by about 2 %. Although the value seems to be low at first glance, it induces its influence on the CH_4 conversion as a key parameter. Looking again at Fig. 9(a), a reduction of 57 % in the conversion is found. Although the only reason of conversion reduction is not the attenuation of the adsorption mechanism, its effectiveness cannot be neglected at all.

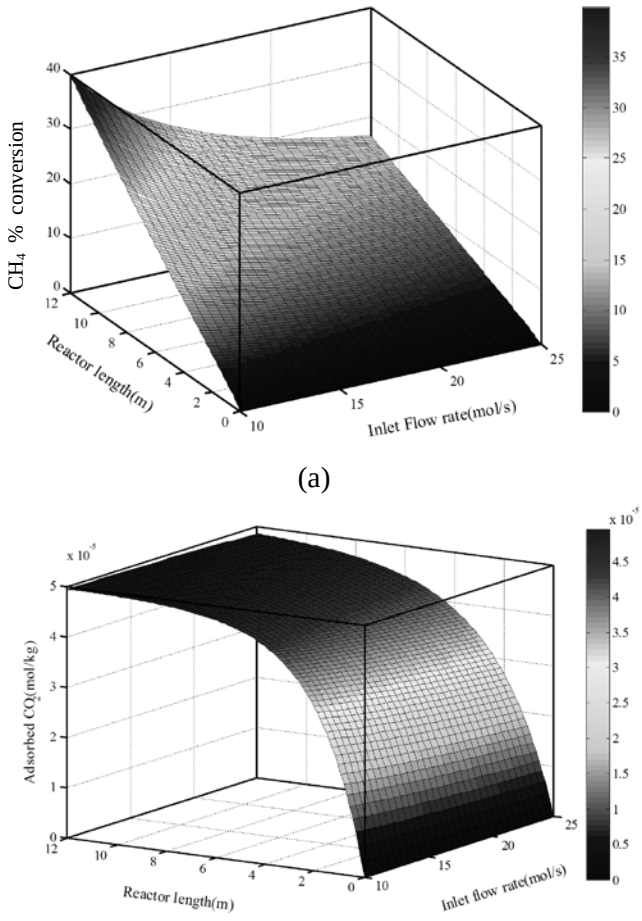

Figure 10. (a) CH_4 conversion and (b) concentration of CO_2 on the adsorbents along the MR length in different total flow rates.

In this part, true Pareto optimal solutions and NSGA-II algorithm are compared for both TNK and KUR test problems. As seen in Fig. 11 (a) and (b), black curves of NSGA-II algorithm joined red lines of true Pareto front and covered the entire discontinuous domain on the true Pareto front for both test problems.

Results of the other case studies are plotted in Fig. 12(a-c). All points on each curve present an optimal solution, and the curves are called Pareto set. In the first two figures, A and B show the points of single optimization

9.7. Optimization results

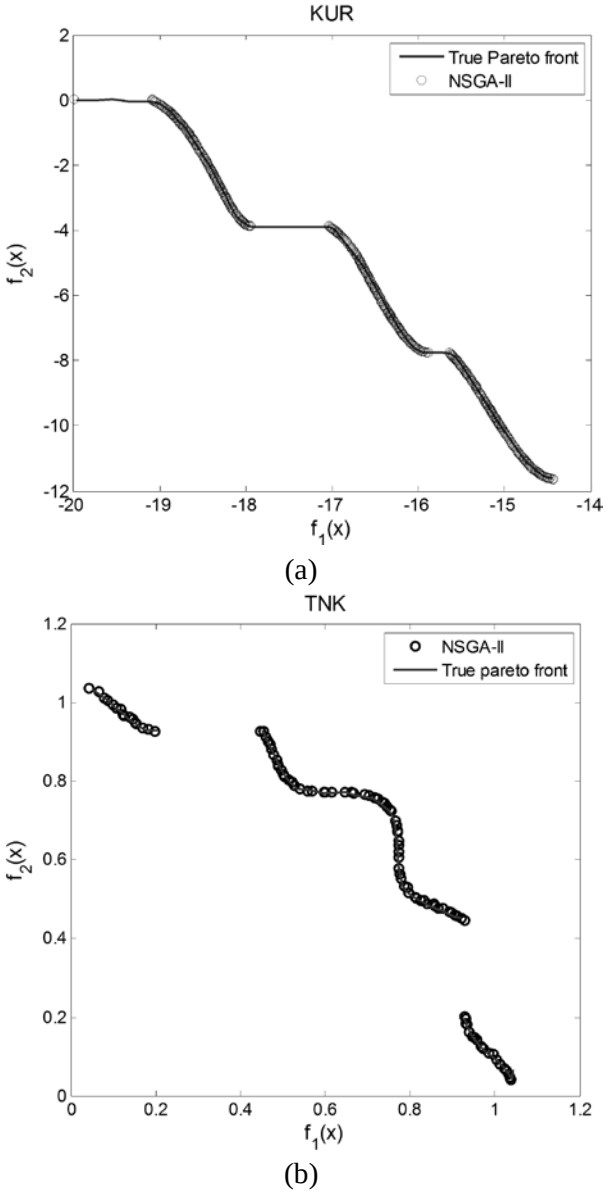

Figure 11. Comparison of true Pareto optimal solutions with those obtained using the NSGA-II algorithm for (a) TNK test problem and (b) KUR.

on each Pareto set. At A, OF_1 is at its minimum value but OF_3 is in its maximum amount, in contrast to B. But as discussed earlier, achieving an optimum condition in which optimizing both objectives is considered simultaneously is more efficient. Thus, A´ and B´ are assigned to the figures. These points and the others located between them are similarly good (non-dominating or non-inferior) and have approximate optimum values of both CH_4 conversion and CO selectivity (Fig. 14a), and H_2/CO ratio and CO selectivity (Fig. 14b). Optimum values of the midpoints are reported in Table 5 (second case study) and 6 (third case study) for decision variables and three objectives. It should be noted that points of the CR and GFSFBR conditions are set in the figures to clearly display the superiority of the conditions obtained by MO.

Also, the 3D plot of three objective functions is shown in Fig. 12(c).

Figure 13(a-g) illustrates the distribution of seven mentioned decision variables for the optimal solutions. The dispersion and accumulation of points are observed in figures retrieved from the conflicting nature of the decision variables. Regions in which density of points is high show the optimum intervals for each variable. According to the figures, optimum intervals of decision variables are approximately as follows:

$$780 < T_g < 800 \qquad (K)$$

$$843 < T_s^{'} < 850 \qquad (K)$$

$$6\times10^{-4} < S < 6.5\times10^{-4} \qquad (\frac{kg}{m^2.s})$$

$$450 < d_s < 500 \qquad (\mu m)$$

$$2000 < F_t < 2100 \qquad (\frac{mol}{s})$$

$$31 < P < 31.5 \qquad (bar)$$

$$0.475 < {H_2}/{CH_4} < 0.48$$

In order to improve the performance of GFSFBR model, it is suggested to operate the proposed reactor in the optimal conditions mentioned above.

Table 5
Optimum values of operating conditions and objective functions for the midpoints between A´and B´.

Tg	Ts	S	ds	Ft	Pt	H/CO	OF_1	OF_2	OF_3
788.0564	849.2684	0.000618	486.734	2700.756	31.23066	0.476	34.61514	0.027349	14.94116
791.1224	848.062	0.000612	481.1366	2732.54	31.18906	0.475839	34.34266	0.027005	15.06143
786.928	836.3375	0.000623	481.2636	2897.132	31.2657	0.4776	31.80129	0.023708	16.40945
786.1529	843.7978	0.00057	455.549	2870.1	31.8478	0.476514	31.98569	0.024057	16.22169
783.9987	841.2394	0.000587	469.9619	2805.955	31.18505	0.476117	32.84853	0.025006	15.85284
784.2622	850.0448	0.000607	475.893	2868.068	31.04697	0.475535	32.03259	0.02396	16.30758
784.1171	854.5956	0.000604	465.9156	2902.621	31.04894	0.475054	31.56256	0.023379	16.57086
784.7253	842.8583	0.000602	468.4288	2773.546	31.24829	0.477992	33.37333	0.025664	15.58774
780.9751	832.2529	0.000537	434.0607	2874.778	31.89732	0.473993	31.55638	0.023521	16.46343
790.4208	843.5056	0.000563	463.495	2789.858	31.30344	0.473341	33.40958	0.025846	15.48749
790.6363	838.164	0.000586	481.4952	2865.967	31.22642	0.47761	32.45452	0.024555	16.02886
788.4167	838.885	0.000613	479.5106	2811.096	31.24481	0.477378	33.06138	0.025305	15.7226
786.9823	839.1889	0.00063	534.4786	2811.69	31.31073	0.47761	32.93311	0.025161	15.77584
784.7205	841.1306	0.00059	482.4189	2713.388	31.25084	0.476614	34.22146	0.026801	15.14535
790.0993	843.049	0.0006	490.079	2694.508	31.31814	0.474966	34.79893	0.027654	14.82101
785.8585	849.4541	0.0006	469.7778	2680.518	31.07075	0.475472	34.81308	0.027565	14.87513
793.5929	844.1533	0.000619	478.7347	2785.831	31.26829	0.477347	33.73939	0.026224	15.34953
788.3408	843.7978	0.00057	455.549	2870.1	31.8478	0.476514	32.12328	0.024246	16.13428
791.1306	851.5393	0.000587	456.3766	2876.973	31.1398	0.475593	32.336	0.024406	16.09462
787.516	835.4858	0.000621	465.1782	2738.327	31.48443	0.478163	34.01767	0.026561	15.22721
783.5188	847.9808	0.000558	463.6195	2914.859	31.06894	0.474951	31.3567	0.023139	16.6789
791.4332	842.9171	0.000592	484.581	2782.52	31.31962	0.475583	33.60493	0.02608	15.39899
785.1358	834.455	0.000611	461.9053	2755.597	31.64071	0.474882	33.52916	0.025988	15.43424
793.0786	844.634	0.000594	477.0392	2758.634	31.2344	0.47669	34.09105	0.026689	15.17329
783.1874	834.6718	0.000563	506.4173	2813.003	31.4341	0.47359	32.5904	0.024782	15.92168
790.2486	842.9643	0.000553	459.4786	2758.327	31.30693	0.476005	33.89477	0.026437	15.26686
786.1088	836.311	0.000593	459.7323	2742.846	31.4531	0.476759	33.8453	0.026345	15.30795
787.4099	842.0635	0.000597	467.6012	2795.795	31.25321	0.477105	33.21042	0.025491	15.64852
787.9951	847.0017	0.000626	479.1978	2798.836	31.30783	0.475336	33.16119	0.025467	15.65037
783.9987	841.2394	0.000587	469.9619	2822.365	31.18505	0.476117	32.62032	0.024717	15.97389
781.8425	833.0353	0.000593	456.8278	2899.396	31.65674	0.476713	31.36873	0.023216	16.62456
786.226	842.5612	0.000602	476.8279	2855.802	31.29442	0.475053	32.26226	0.024319	16.13105
787.7582	849.3634	0.000611	469.92	2838.533	31.17271	0.478599	32.67995	0.024779	15.94963
783.5188	849.1081	0.000603	463.6195	2910.956	31.06894	0.474951	31.4114	0.023193	16.65774

Table 6
Optimum values of operating conditions and objective functions for the midpoints between A´and B´.

Tg	Ts	S	ds	Ft	Pt	H/C	F_1	F_2	F_3
788.0564	849.2684	0.000618	486.734	2700.756	31.23066	0.476	34.61514	0.027349	14.94116
791.1224	848.062	0.000612	481.1366	2732.54	31.18906	0.475839	34.34266	0.027005	15.06143
784.7205	841.1306	0.00059	482.4189	2713.388	31.25084	0.476614	34.22146	0.026801	15.14535
790.0993	843.049	0.0006	490.079	2694.508	31.31814	0.474966	34.79893	0.027654	14.82101
785.8585	849.4541	0.0006	469.7778	2680.518	31.07075	0.475472	34.81308	0.027565	14.87513
787.516	835.4858	0.000621	465.1782	2738.327	31.48443	0.478163	34.01767	0.026561	15.22721
793.0786	844.634	0.000594	477.0392	2758.634	31.2344	0.47669	34.09105	0.026689	15.17329
790.2486	842.9643	0.000553	459.4786	2758.327	31.30693	0.476005	33.89477	0.026437	15.26686
786.1088	836.311	0.000593	459.7323	2742.846	31.4531	0.476759	33.8453	0.026345	15.30795

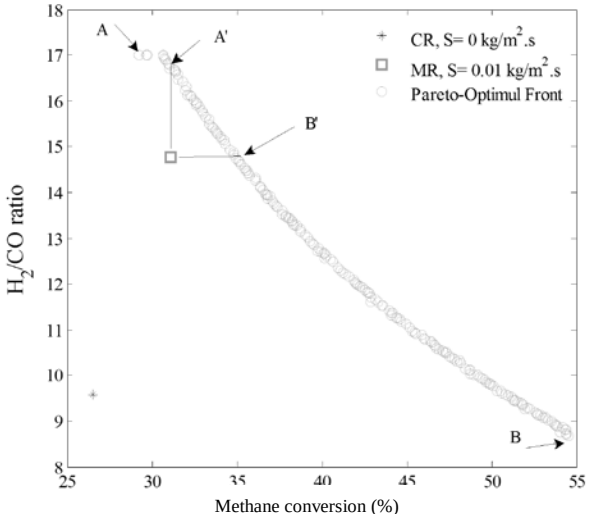

(a)

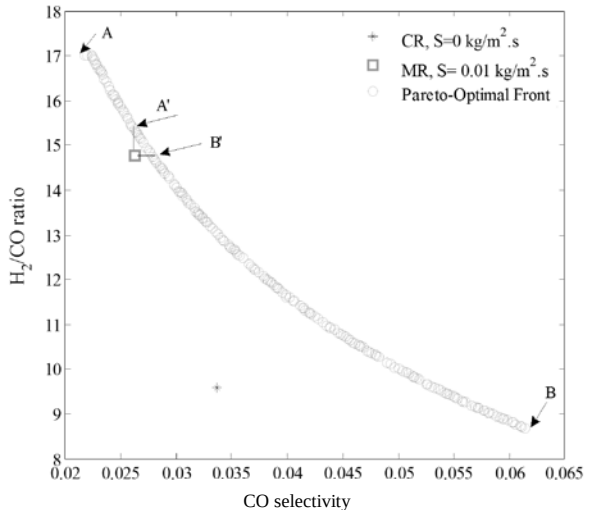

(b)

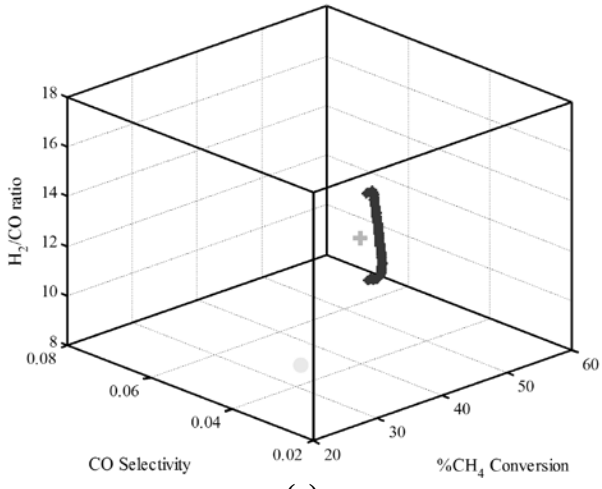

(c)

Figure 12. (a) Preto optimal fronts for (a) OF_1 versus OF_3, (b) OF_2 versus OF_3 and (3) all three objective functions.

10. Conclusions

The possibility of enhancing productivity of an industrial steam-methane reforming process was studied, employing the concept of sorption-enhanced reaction. A mathematical model of a GFSFBR was developed by considering plug flow patterns for moving phases (pre-reformed gas and adsorbents). It was observed that in the presence of flowing CO_2 adsorbent particles, the process was

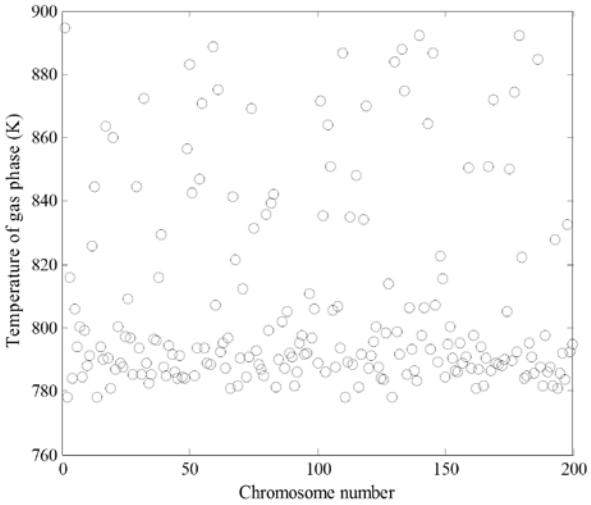
Temperature of gas phase (K)
900
880
860
840
820
800
780
760
0
50
100
150
200
Chromosome number

(a)

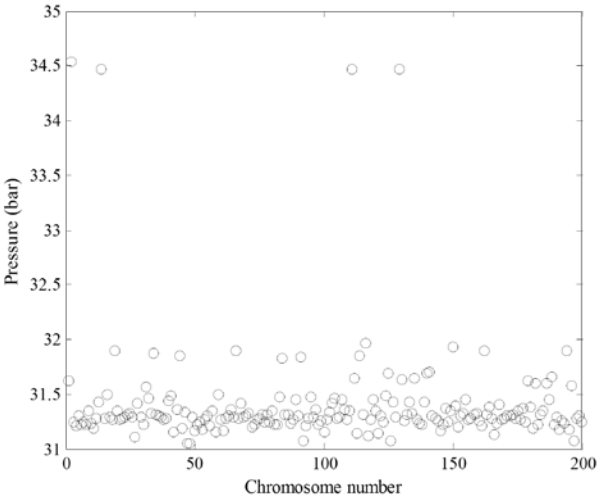
Pressure (bar)
35
34.5
34
33.5
33
32.5
32
31.5
31
0
50
100
150
200
Chromosome number

(d)

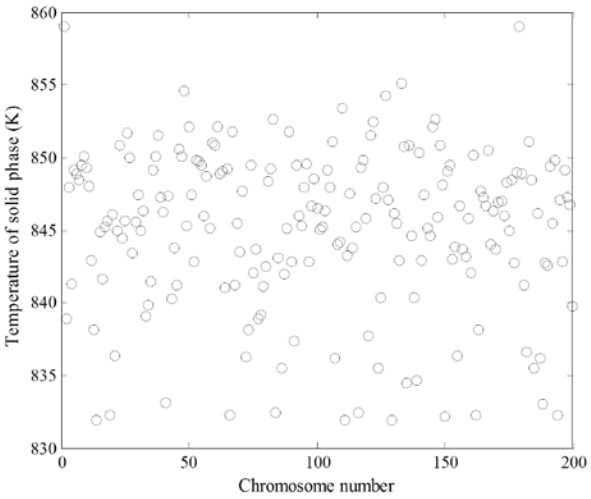
Temperature of solid phase (K)
860
855
850
845
840
835
830
0
50
100
150
200
Chromosome number

(b)

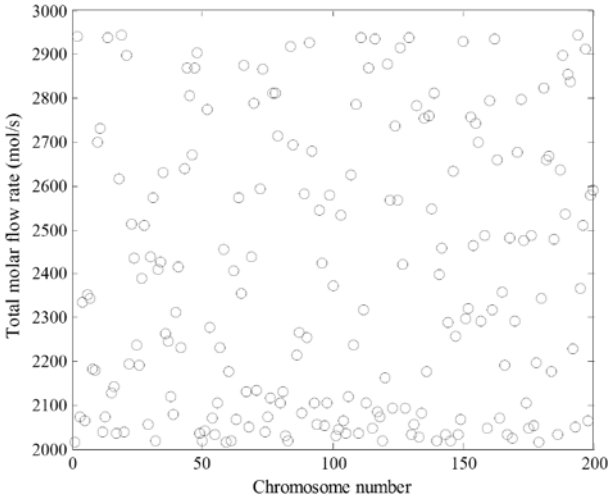
Total molar flow rate (mol/s)
3000
2900
2800
2700
2600
2500
2400
2300
2200
2100
2000
0
50
100
150
200
Chromosome number

(e)

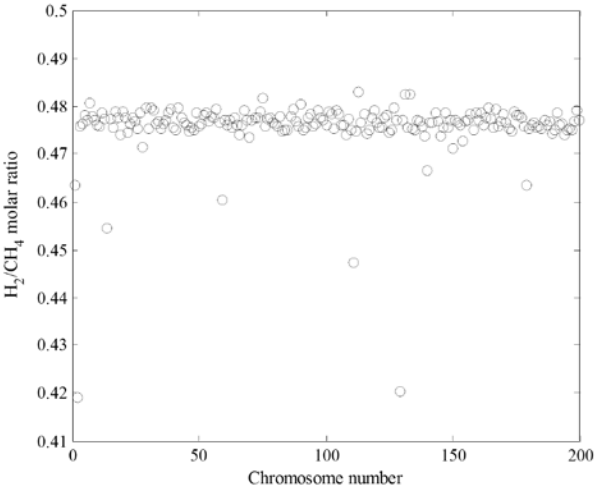
H_2/CH_4 molar ratio
0.5
0.49
0.48
0.47
0.46
0.45
0.44
0.43
0.42
0.41
0
50
100
150
200
Chromosome number

(c)

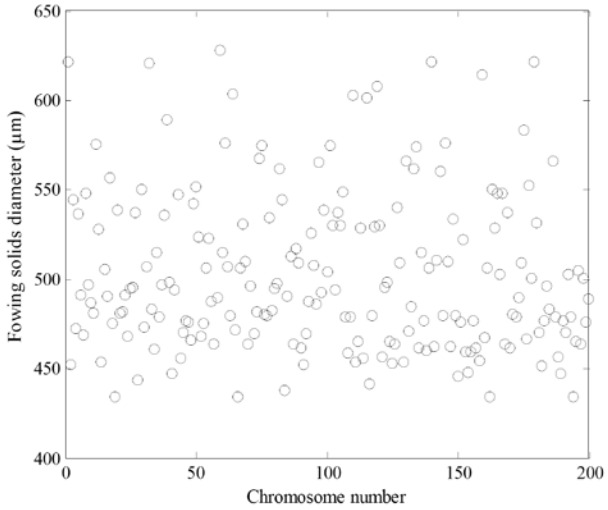
Fowing solids diameter (μm)
650
600
550
500
450
400
0
50
100
150
200
Chromosome number

(f)

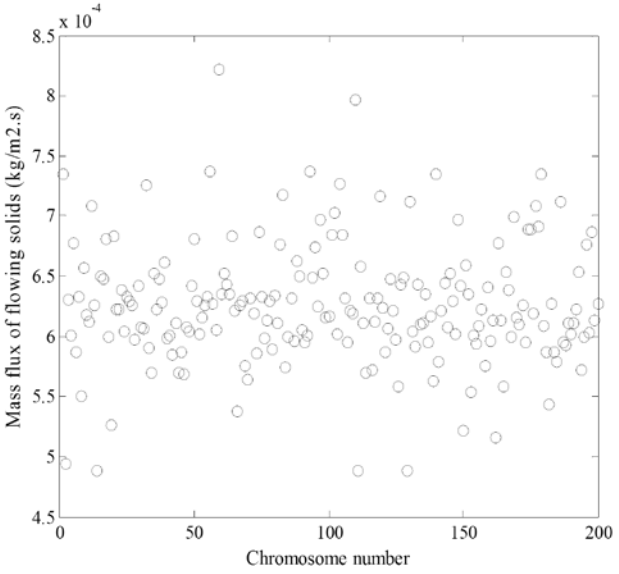

(g)

Figure 13. Distribution of decision variables (T_g, T'_s, S, d_s, F_t, P, H_2/CH_4).

improved owing to higher methane conversion and hydrogen production together with lower CO_2 emission. Moreover, variation of some operating parameters was investigated along the axial direction of the reactor to analyze process sensitivity. Finally, results showed that higher mass flux of the adsorbents and inlet temperature as well as lower adsorbents' diameter, inlet pressure and gas flow rate not only enhance methane conversion and hydrogen production, but also ameliorate adsorption of carbon dioxide. Multi-objective optimization was also performed on the model, using non-dominated sorting genetic algorithm-II. Following the purpose of maximizing three objective functions of CH_4 conversions, CO selectivity and H_2/CO ratio, optimal operating conditions were reported in specific intervals. It can be claimed that this is the main strength of this approach.

Nomenclature

A_c	cross section area of each tube [m^2].
A_r	Archimedes number for flowing solid particles.
a'_s	specific surface area of flowing solid [m^2/m^3].
b_{CO_2}	Langmuir model constant for component CO_2 [Pa^{-1}].
C_d	drag coefficient.
Cp'_g	specific heat of the gas at constant pressure [J/ (mol.K)].
Cp'_s	specific heat of the flowing solid at constant pressure [J/(mol.K)].
D_i	tube inside diameter [m].
D_{ij}	binary diffusion coefficient of component i in j [m^2/ s].
D_{im}	diffusion coefficient of component i in the mixture [m^2/s].
d_{eq}	equivalent diameter of packing particles.
d_s	catalyst diameter [m].
d'_s	flowing solid diameter [m].
F_i	molar flow of species i [mol/s].
F_t	total molar flow per tube [mol/s].
ΔH_{ads}	specific heat of adsorption [J/mol].
$\Delta H_{f,i}$	enthalpy of formation of component i [J/mol].
h'_f	gas–solid heat transfer coefficient [W/(m^2 K)].
K_g	conductivity of the gas phase [W.m/K].
k'_g	gas–solid mass transfer coefficient [m/s].
L	length of reactor [m].
m_{CO_2}	Langmuir model constant for component CO_2 [mol/kg].
M_i	molecular weight of component i [g/mol].
P	total pressure [bar].
q_{CO_2}	concentration of CO_2 adsorbed in flowing solids [mol/kg].
$q^*_{CO_2}$	equilibrium solid-phase concentration [mol/ kg].

R universal gas constant [J/(mol K)].

Re'_s Reynolds number of flowing solid.

r_i reaction rate of component i [mol/(kg s)].

S mass flux of flowing solids [kg/(m^2.s)].

T bulk gas phase temperature [K].

T'_s temperature of flowing solid [K].

u_g superficial gas velocity [m/s].

u_r relative velocity for co-current flow of gas and flowing solid [$u_r = u_g - u'_s$].

u'_s real flowing solid velocity [$S/\rho'_s\beta$].

x molar composition.

X methane conversion.

y_i mole fraction of component i in the fluid phase [mol/mol].

Z axial reactor coordinate [m].

Greek letters

β flowing solids holdup [$\beta = \beta_d + \beta_s$].

ε void fraction of catalytic bed [m^3/m^3].

ε' void fraction corrected due to presence of the flowing solids ($\varepsilon' = \varepsilon - \beta$) [m^3/m^3].

υ_{ci} critical volume of component i [m^3/mol].

μ dynamic viscosity.

ρ_B catalytic bed density [kg/m^3].

ρ_g gas density [kg/m^3].

ρ'_S flowing solids density [kg/m^3].

ϕ sphericity of packed bed element.

References

[1] Wang, F., Qi, B., Wang, G. and Li, L., "Methane steam reforming: Kinetics and modeling over coating catalyst in micro-channel reactor", Int. J. Hydrog. Energy, **38** (14), 5693 (2013).

[2] Bej, B., Pradhan, N.C. and Neogi, S., "Production of hydrogen by steam reforming of methane over alumina supported nano-NiO/SiO_2 catalyst", Catal. Today, **207**, 28 (2013).

[3] Song, C., Liu, Q., Ji, N., Kansha, Y. and Tsutsumi, A., "Optimization of steam methane reforming coupled with pressure swing adsorption hydrogen production process by heat integration", Appl. Energy, **154**, 392 (2015).

[4] Barelli, L., Bidini, G., Gallorini, F. and Servili, S., "Hydrogen production through sorption-enhanced steam methane reforming and membrane technology: A review", Energy, **33** (4), 554 (2008).

[5] Simpson, A.P. and Lutz, A.E., "Exergy analysis of hydrogen production via steam methane reforming", Int. J. Hydro. Energy, **32** (18), 4811 (2007).

[6] Hufton, J.R., Mayorga, S. and Sircar, S., "Sorption-enhanced reaction process for hydrogen production", AIChE J., **45** (2), 248 (1999).

[7] Westerterp, K.R. and Kuczynski, M., "A model for a counter current gas-solid-solid trickle flow reactor for equilibrium reactions", Chem. Eng. Sci., **42** (8), 1871 (1987).

[8] Ding, Y. and Alpay, E., "Equilibria and kinetics of CO_2 adsorption on hydrotalcite adsorbent", Chem. Eng. Sci., **55** (17), 3461 (2000).

[9] Gunduz, S. and Dogu, T., "Sorption enhanced ethanol reforming of ethanol over Ni- and Co-incorporated MCM-41 type catalysts", Ind. Eng. Chem. Res., **51** (26), 8796 (2012).

[10] Bayat, M., Hamidi, M., Dehghani, Z., Rahimpour, M.R. and Shariati, A.,

"Hydrogen/methanol production in a novel multifunctional reactor with in situ adsorption: Modeling and optimization", Int. J. Energy Res., **38** (8), 978 (2014).

[11] Dehghani, Z., Bayat, M. and Rahimpour, M.R., "Sorption-enhanced methanol synthesis: Dynamic modeling and optimization", J. Taiwan. Inst. Chem. Eng., **45** (4), 1490 (2014).

[12] Bayat, M., Dehghani, Z. and Rahimpour, M.R., "Sorption-enhanced methanol synthesis in a dual-bed reactor: Dynamic modeling and simulation", J. Taiwan. Inst. Chem. Eng., **45** (5), 2307 (2014).

[13] Van, D.D. and Staatsmijnen, D., French Pat. 978287, Lumburg, (1948).

[14] Fourth methanol documents of Lurgi. Zagros Petrochemical Complex in Assaluyeh, Iran.

[15] Xiu, G.H., Lia, P. and Rodrigues, A.E., "Sorption-enhanced reaction process with reactive regeneration", Chem. Eng. Sci., **57** (18), 3893 (2002).

[16] Arab Aboosadi, Z., Rahimpour, M.R. and Jahanmiri. A., "A novel integrated thermally coupled configuration for methane-steam reforming and hydrogenation of nitrobenzene to aniline", Int. J. Hydrog. Energy, **36** (4), 2960 (2011).

[17] Mbodji, M., Commenge, J.M., Falk, L., Di Marco, D., Rossignol, F., Prost, L., Valentin, S., Joly, R. and Del-Gallo, P., "Steam methane reforming reaction process intensification by using a millistructured reactor: Experimental setup and model validation for global kinetic reaction rate estimation", Chem. Eng. J., **207-208**, 871 (2012).

[18] Gosiewski, K., Bartmann, U., Moszczynski, M. and Mleczko, L., "Effect of the intraparticle mass transport limitations on temperature profiles and catalytic performance of the reverse-flow reactor for the partial oxidation of methane to synthesis gas", Chem. Eng. Sci., **54** (20), 4589 (1999).

[19] Ranz, W.E. and Marshall. W.R., "Evaporation from drops II", Chem. Eng. Prog., **48** (141), 173 (1952).

[20] Claus, G., Vergnes, F. and Le Goff, P., "Hydrodynamic study of gas and solid flow through a screen-packing", Can. J. Chem. Eng., **54** (3), 143 (1976).

[21] Predojevic, Z.J., Lj Petrovic, D. and Dudukovic, A.P., "Pressure drop in a countercurrent gas−flowing solids−packed bed contactor", Ind. Eng. Chem. Res., **40** (25), 6039 (2001).

[22] Benali, M. and Shakourzadeh-Bolouri, K., "The gas-solid-solid packed contactor: Hydrodynamic behaviour of counter-current trickle flow of coarse and dense particles with a suspension of fine particles", Int. J. Multiphase Flow, **20** (1), 161 (1994).

[23] Nikacevic, N., Jovanovic, M. and Petkovska, M., "Enhanced ammonia synthesis in multifunctional reactor with in-situ adsorption", Chem. Eng. Res. Des., **89** (4), 398 (2011).

[24] Spasic, A.M. and Hsu, J.P., Finely dispersed particles. micro-, nano-, and atto-engineering, CRC Press, Taylor & Francis, Boca Raton, p.371 (2006).

[25] Perry, R.H. and Green, D.W., Perry's

Chemical Engineers' Handbook, 8th ed., McGraw-Hill, Singapore, p.420 (2008).

[26] Cussler, E.L., Diffusion: Mass transfer in fluid systems, Cambridge University Press, (1984).

[27] Wilke, C.R. "Estimation of liquid diffusion coefficients", Chem. Eng. Prog., **45** (3), 218 (1949).

[28] Reid, R.C., Sherwood, T.K. and Prausnitz, J., The properties of gases and liquids, 3rd ed., McGraw-Hill, New York, (1977).

[29] Dudukovic, A.P., Nikacevic, N.M., Lj Petrovic, D. and Predojevic, Z.J. "Solids holdup and pressure drop in gas-flowing solids-fixed bed contactors", Ind. Eng. Chem. Res., **42** (12), 2530 (2003).

[30] Perry, R.H. and Green, D.W., Perry's Chemical Engineers' Handbook, 8th ed., McGraw-Hill, Singapore, p.433 (2008).

[31] Hartig, F. and Keil, F.J. "Large-scale spherical fixed bed reactor: Modeling and optimization", Ind. Eng. Chem. Res., **32** (3), 424 (1993).

[32] Rajesh, J.K., Gupta, S.K., Rangaiah, G.P. and Ray, A.K., "Multi-objective optimization of steam reformer performance using genetic algorithm", Ind. Eng. Chem. Res., **39** (3), 706 (2000).

[33] Luo, X., Hu, J., Zhao, J., Zhang, B., Chen, Y. and Mo, S., "Multi-objective optimization for the design and synthesis of utility systems with emission abatement technology concerns", Appl. Energy, **136**, 1110 (2014).

[34] Deb, K., Pratap, A., Agarwal, S. and Meyarivan, T., "A Fast and elitist multi-objective genetic algorithm: NSGA-II", IEEE Trans. Evol. Comput., **6** (2), 182 (2002).

[35] Bayat, M., Dehghani, Z. and Rahimpour, M.R., "Dynamic multi-objective optimization of industrial radial-flow fixed-bed reactor of heavy paraffin dehydrogenation in LAB plant using NSGA-II method", J. Taiwan. Inst. Chem. Eng., **45** (4), 1474 (2014).